Contribution from the National Institute for Research in Inorganic Materials, 1-1 Namiki, Sakura-mura, Niihari-gun, Ibaraki 305, Japan

# Layered Hydrous Titanium Dioxide: Potassium Ion Exchange and Structural Characterization

TAKAYOSHI SASAKI,* MAMORU WATANABE, YŪ KOMATSU, and YOSHINORI FUJIKI

*Received August 22, 1984*

Potassium ion exchange on layered hydrous titanium dioxide ($H_2Ti_4O_9 \cdot 1.2H_2O$), which is obtained from potassium tetratitanate ($K_2Ti_4O_9$), has been studied by examining the titration curve in relation to the structural change of the material. Structural characterization has also been performed for layered hydrous titanium dioxide and its potassium ion exchanged phases. The material has almost the same sheet structure of $[Ti_4O_9^{2-}]_n$ as that of potassium tetratitanate, in which hydronium ions and hydroxylated protons are situated as exchangeable ones. The ion exchange proceeds stepwise through four stages (0–25, 25–50, 50–70, and 70–98% conversion), indicating that potassium ions replace the exchangeable protons one by one. During the process four solid phases appeared with different interlayer distances and cation/water contents: one-fourth-exchanged phase, $K_{0.5}H_{1.5}Ti_4O_9 \cdot 0.6H_2O$; half-exchanged phase, $KHTi_4O_9 \cdot 0.5H_2O$; approximately three-fourths-exchanged phase, $K_{1.4}H_{0.6}Ti_4O_9 \cdot 1.2H_2O$; and fully exchanged phase, $K_2Ti_4O_9 \cdot 2.2H_2O$. The study of the unit cell dimensions of these phases indicates that the ion exchange takes place accompanied by a contraction/expansion of interlayer distances and a shift of adjacent sheets in relation to each other along the *c* axis. A lattice type change occurred during the process, which is considered to be due to the arrangement of potassium ions and/or water molecules incorporated in the interlayer space. A structural model is proposed for the fully exchanged phase in which interlayered potassium ions and water molecules occupy the sites arranged in a double row and shifted above and below the levels at $y = 0$ and $^1/_2$. Models for the other ion-exchanged phases are also proposed to interpret the ion-exchange mechanism from a structural aspect.

## Introduction

Hydrous titanium dioxide has been studied extensively as an inorganic ion exchanger since it possesses high selectivity of sorption toward certain metal ions, e.g. uranyl ion in sea water.[1-8] Three types of hydrous titanium dioxide have been reported so far: amorphous, anatase-type, and rutile-type material.[5,6] But they do not show reproducible sorption characteristics because of poor crystallinities.

A new type of hydrous titanium dioxide with layer structure has been prepared as a derivative of potassium tetratitanate.[9-11] This material, which is termed "layered hydrous titanium dioxide", exhibits reproducible ion exchange and intercalating abilities. Tournoux and his co-workers have analyzed the crystal structure of thallium tetratitanate, which is isomorphous with alkali-metal tetratitanates.[12,13] Figure 1 shows the idealized representation of the crystal structure of alkali-metal tetratitanate. The basic framework is built up from a structure unit of four $TiO_6$ octahedra arranged in a line by means of edge sharing. The units are combined with each other above and below to form a zigzag string of octahedra. The string is then joined with other strings by corner sharing to make a staggered sheet. These sheets are stacked in the direction of the *a* axis in such a way that they shift by $b/2$ along the *b* axis. Nonuniform interlayer space is generated by such an arrangement (see Figure 1b). The narrow–wide region repeats every *b* (ca. 3.8 Å), and alkali-metal ions are situated in the wider region.

The interlayered potassium ions are very easily extracted by treatment with acid solutions.[9-11] Layered hydrous titanium dioxide is obtained by extracting potassium ions completely. This material is interesting because it is one of the first hydrous metal oxides with layer structure that act as ion exchangers.

We have reported the preparation of this material in a fibrous form that is very useful when it is used in a column or as an ion-exchange paper.[9] We have studied the sorption of microquantities of some metal ions and reported that considerably large differences in the affinities toward metal ions were observed in comparison with those of other inorganic ion exchangers and organic ion-exchange resins.[14-16] We have also proposed that this material can be employed to remove and immobilize dangerous nuclides such as cesium and strontium in a high-level radioactive waste solution.[17,18]

The data for the titration behavior and the crystal structure of the exchanger are indispensable to understand the ion-exchange mechanism. There have been few reports dealing with such points except for the papers by Marchand et al.[10] and by Izawa et al.[11] However, the data appearing in their papers do not coincide with each other and are not enough to discuss the ion-exchange mechanism. Izawa et al. have reported the structural data for layered hydrous titanium dioxide and its *n*-alkylammonium complexes.[11,19] But the lattice constants they obtained seem to be unreasonable because the value for the *c* axis is too short for a diagonal length of four $TiO_6$ octahedra. This length has been reported to be 12 ± 0.1 Å for several other titanates with identical arrangement of octahedra.[10,13] Thus, we carried out the characterization of layered hydrous titanium dioxide and its potassium ion exchanged phases to obtain accurate structural data. On the basis of these data, we attempted to interpret and discuss the ion-exchange process.

This paper describes the potassium ion exchange process on layered hydrous titanium dioxide. This material and its potassium ion exchanged phases are characterized mainly from a structural viewpoint. The ion-exchange mechanism is discussed by taking into account the titration curve and the structural change of the exchanger. The tentative structural models for some of the ion-exchanged phases are put forward in relation to the ion-exchange mechanism.

(1) Amphlett, C. B.; McDonald, L. A.; Redman, M. *J. Inorg. Nucl. Chem.* **1958**, *6*, 236.
(2) Bobyrenko, Yu, Ya.; Dolmatov, Yu. D.; Bragina, M. I. *Zh. Prikl, Khim. (Leningrad)* **1970**, *43*, 1152.
(3) Heitner-Wirguin, C.; Albu-Yaron, A. *J. Inorg. Nucl. Chem.* **1966**, *28*, 2379.
(4) Levi, H. W.; Schiewer, E.; *Radiochim. Acta* **1966**, *5*, 126.
(5) Abe, M.; Ito, T. *Nippon Kagaku Zasshi* **1965**, *86*, 1259.
(6) Abe, M.; Tsuji, M.; Qureshi, S. P.; Uchikoshi, H. *Chromatographia* **1980**, *13*, 626.
(7) Keen, N. J. *J. Br. Nucl. Energy Soc.* **1968**, *7*, 178.
(8) Ogata, N. *Nihon Genshiryoku Gakkaishi* **1971**, *13*, 121.
(9) Ohta, N.; Fujiki, Y. *Yogyo Kyokaishi* **1980**, *88*, 1.
(10) Marchand, R.; Brohan, L.; Tournoux, M. *Mater. Res. Bull.* **1980**, *15*, 1129.
(11) Izawa, H.; Kikkawa, S.; Koizumi, M. *J. Phys. Chem.* **1982**, *86*, 5023.
(12) Verbaere, A.; Tournoux, M. *Bull. Soc. Chim. Fr.* **1973**, 1237.
(13) Dion, M.; Piffard, Y.; Tournoux, M. *J. Inorg. Nucl. Chem.* **1978**, *40*, 917.
(14) Komatsu, Y.; Fujiki, Y.; Sasaki, T. *Bunseki Kagaku* **1982**, *31*, E225.
(15) Komatsu, Y.; Fujiki, Y.; Sasaki, T. *Bunseki Kagaku* **1983**, *32*, E33.
(16) Sasaki, T.; Komatsu, Y.; Fujiki, Y. *Sep. Sci. Technol.* **1983**, *18*, 49.
(17) Fujiki, Y.; Komatsu, Y.; Sasaki, T.; Ohta, N. *Nippon Kagaku Kaishi* **1981**, 1656.
(18) Sasaki, T.; Komatsu, Y.; Fujiki, Y. *Chem. Lett.* **1981**, 957.
(19) Izawa, H.; Kikkawa, S.; Koizumi, M. *Polyhedron* **1983**, *2*, 741.

0020-1669/85/1324-2265$01.50/0 

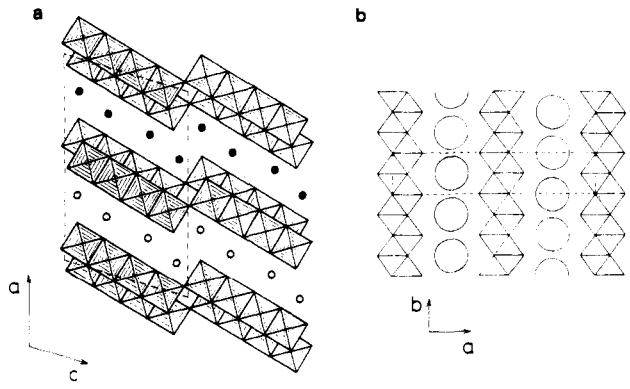


**Figure 1.** Idealized representation of crystal structure of alkali-metal tetratitanate. (a) Projection along (010): closed circles, alkali-metal ions at $y = {}^1/_2$; open circles, alkali-metal ions at $y = 0$. (b) Projection along (001): circles, alkali-metal ions.

## Experimental Section

**Reagents.** The titanium dioxide used was of 99.98% purity. All the other chemicals were of reagent grade. Potassium hydoxide solution was standardized against potassium hydrogen phthalate. Distilled, deionized water was used throughout the experiment.

**Preparation of the Materials.** Potassium tetratitanate in a fibrous form was grown from a $K_2MoO_4$ flux melt containing a 3/1 $K_2O$–$TiO_2$ mixture by the slow-cooling method.[20] Layered hydrous titanium dioxide was obtained by extracting the interlayered potassium ions as follows: About 15 g of potassium tetratitanate was placed in a glass column (2.5-cm i.d.) and treated with a 1 mol $dm^{-3}$ hydrochloric acid solution until potassium ions in the effluent were negligible ($<1 \times 10^{-5}$ mol $dm^{-3}$). Then the solid was washed with water to remove excessive acid until the pH of the effluent was 5–6. The resulting product was dried over a saturated NaCl solution (relative humidity 70%) to a constant weight.

**Equilibrium Studies.** The titrations were carried out by a batch procedure; 0.2 g of the material was shaken with 0.02 $dm^3$ of a 0.1 mol $dm^{-3}$ KCl–KOH solution at 25 ± 0.5 °C. The KCl/KOH molar ratio was varied from 0.1/0.0 to 0.0/0.1. The equilibration time was 4 days. After the equilibrium was attained, the supernatant solutions were analyzed for their pH values and metal ion contents. The pH values were measured by a TOA HM-20E digital pH meter and metal ion contents by a Hitachi 180-80 atomic absorption spectrophotometer. The metal ion uptake was calculated from the difference between initial and final concentrations of the solution. The solid was filtered off, washed, and dried over a saturated NaCl solution.

**Characterization of the Solid Phases.** The solid phases were characterized by chemical analysis, IR spectroscopy, and powder X-ray diffractometry. The chemical analysis was carried out as follows: The solid phases were dissolved by concentrated sulfuric acid and ammonium sulfate with heating. The potassium ion content was determined by atomic absorption spectrophotometry. The titanium was determined gravimetrically by using a cupferron as a precipitant. The water content was deduced by measuring the weight loss at 800 °C.

The IR spectra were taken by the standard KBr disk technique with a Hitachi infrared spectrometer.

The X-ray powder diffraction patterns were obtained by using silicon or titanium dioxide (rutile) as an internal standard on a PW-1130 type Philips diffractometer with Ni-filtered Cu Kα radiation (λ = 1.5405 Å). The data were collected over the $2\theta$ range of 4–50° at a scan rate of 1/16° $min^{-1}$. The unit cell dimensions were refined by the least-squares method (program name APPLEMAN II).

## Results and Analysis

**Characterization of Layered Hydrous Titanium Dioxide.** From the chemical analysis, layered hydrous titanium dioxide was confirmed to contain a negligible amount of potassium ions (<1.0 mg/g material) and 1.2 mol of hydrated water per formula weight. Thus the preparation of this material can be formulated as

$$K_2Ti_4O_9 + 2H^+ + 1.2H_2O \rightarrow H_2Ti_4O_9 \cdot 1.2H_2O + 2K^+ \quad (1)$$

The chemical formula, $H_2Ti_4O_9 \cdot 1.2H_2O$, means that this material has a theoretical ion-exchange capacity of 5.57 mequiv/g. The material has a fibrous form with white color. The size of a fiber was 1 mm in length × 0.01 mm in diameter, on average.

Table I. X-ray Powder Diffraction Data for Layered Hydrous Titanium Dioxide

| $h\ k\ l$ | $d_{calcd}$, Å | $d_{obsd}$, Å | intens |
|---|---|---|---|
| 0 0 1 | 10.99 | 10.98 | vw |
| 2 0 0 | 9.12 | 9.04 | vs |
| 2 0 $\bar{1}$ | 9.06 | | |
| 2 0 1 | 5.93 | 5.93 | vw |
| 2 0 $\bar{2}$ | 5.88 | 5.89 | vw |
| 4 0 $\bar{1}$ | 4.99 | 4.99 | s |
| 4 0 0 | 4.56 | 4.56 | w |
| 2 0 2 | 4.04 | 4.03 | vw |
| 4 0 1 | 3.711 | 3.709 | m |
| 1 1 0 | 3.669 | 3.670 | s |
| 6 0 $\bar{2}$ | 3.286 | 3.284 | m |
| 3 1 0 | 3.189 | 3.187 | m |
| 6 0 $\bar{3}$ | 3.020 | 3.019 | m |
| 4 0 $\bar{2}$ | 2.965 | 2.967 | s |
| 5 1 $\bar{1}$ | 2.728 | 2.728 | vw |
| 6 0 1 | 2.665 | 2.664 | w |
| 6 0 $\bar{4}$ | 2.641 | 2.641 | w |
| 8 0 $\bar{3}$ | 2.429 | 2.428 | m |
| 4 0 $\bar{5}$ | 2.397 | 2.397 | s |
| 2 0 $\bar{5}$ | 2.366 | 2.366 | m |
| 6 0 2 | 2.294 | 2.293 | w |
| 8 0 1 | 2.071 | 2.072 | m |
| 2 0 5 | 1.962 | 1.960 | m |
| 6 0 $\bar{6}$ | 1.960 | | |
| 10 0 $\bar{4}$ | 1.922 | 1.923 | m |
| 0 2 0 | 1.873 | 1.873 | m |
| 2 2 0 | 1.835 | 1.835 | vw |
| 2 2 $\bar{1}$ | 1.834 | | |

The X-ray powder pattern can be indexed as given in Table I by assuming that this material has a *C*-base-centered monoclinic lattice ($C2/m$; $Z = 4$). The obtained lattice constants are $a$ = 19.968 (4) Å, $b$ = 3.746 (1) Å, $c$ = 12.025 (2) Å, and $\beta$ = 114.01 (1)°, where numerals in parentheses give the standard deviation in the last figure.

**Analysis on the Structure of Layered Hydrous Titanium Dioxide.** In order to discuss the crystal structure of layered hydrous titanium dioxide, it is essential to compare the obtained lattice constants with those of potassium tetratitanate: $a$ = 18.25 (1) Å, $b$ = 3.791 (1) Å, $c$ = 12.01 (1) Å, and $\beta$ = 106.4 (1)°.[13] The values for the $b$ and $c$ axes are almost equal to those obtained above, indicating the host framework of $[Ti_4O_9^{2-}]_n$ was not destroyed. In conclusion, layered hydrous titanium dioxide has the same sheet structure as that of potassium tetratitanate except for a slight increase in interlayer distance ($(a/2) \sin \beta = 8.75 \rightarrow 9.12$ Å) and a shift of adjacent sheets in relation to each other along the $c$ axis.

The chemical formula, $H_2Ti_4O_9 \cdot 1.2H_2O$, can roughly be represented as $(H^+,H_3O^+)Ti_4O_9$. This means that the material contains two types of exchangeable protons: one hydronium ion and one proton per chemical formula. This idea is supported chemically by the study of the potassium ion exchange process, as will be described later.

Since the monoclinic unit cell consists of four molecules, it contains four hydronium ions and four protons. In general, protons are supposed to exist as hydroxylated protons attached to the oxygen atom with the highest electronegativity. In this structure, the oxygen atoms designated by arrows in Figure 2 are considered to be the most electronegative because they are not shared between octahedra. Four equivalent unshared oxygen atoms are found in each unit cell and are regarded to make hydroxyl bonds with protons. On the other hand, four hydronium ions exist in the interlayer space to keep open the neighboring sheets (see Figure 2).

The IR data also supported this structural model. Three distinctive bands were observed at 3350, 1620, and 940 $cm^{-1}$. They are assigned to O–H stretching, H–O–H bending, and O–H bending, respectively. This suggests the existence of water and hydroxyl groups in the material.

The ion-exchange reaction is considered to begin with diffusion of metal ions into the solid. Because this material has the layer

(20) Fujiki, Y.; Ohta, N. *Yogyo Kyokaishi* **1980**, *88*, 11.

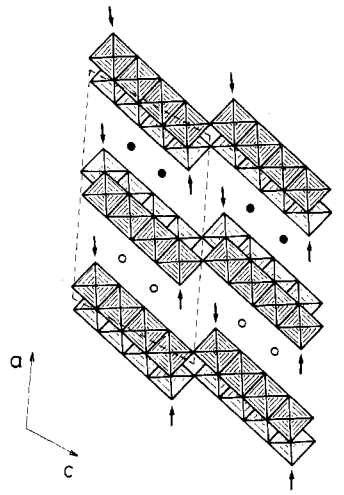


**Figure 2.** Idealized representation of the structure of layered hydrous titanium dioxide. Arrows and circles represent the possible positions of hydroxyl bonds and hydronium ions, respectively.

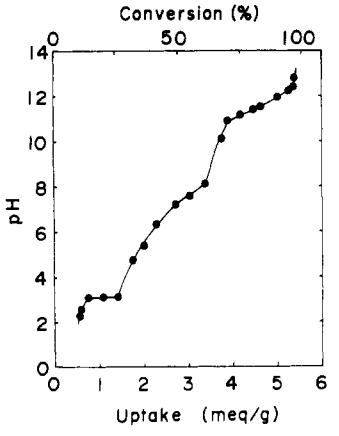


**Figure 3.** Potassium ion titration curve: exchanger, 0.2 g; titrant, 0.02 $dm^3$ of 0.1 mol $dm^{-3}$ KCl–KOH.

structure described above, ingoing ions must move parallel to the sheets. This material does not have a uniform interlayer space; the net spacings of the narrow and wide regions along the *a* axis are approximately estimated as 1.0 and 4.4 Å, respectively, by subtracting the volume of oxygen. Therefore, potassium ions ($r$ = 1.51 Å)[21] are supposed to enter as unhydrated ions along the *c* axis.

**Potassium Ion Exchange Behavior.** Figure 3 shows the potassium ion titration curve of layered hydrous titanium dioxide. After an initial rising portion, the curve had a flat plateau region up to 25% conversion. The pH increased gradually in the region of 25–70% conversion. A pH jump was observed at 70% conversion, and then the curve had a mild-slope region again. The pH value increased steeply at the uptake of 5.45 mequiv/g, which was nearly equal to the theoretical limit.

Figure 4 shows the X-ray powder diffraction patterns of the solids at various loading levels. The X-ray patterns changed continuously up to the loading level of 0.5 mequiv/g. The formation of solid solution in this range means that potassium ions replaced statistically exchangeable protons in the initial phase. This region corresponds with the initial steeply rising portion of the titration curve. Beyond this region, two immiscible solid phases coexisted, which can be seen by the detailed X-ray pattern around the $2\theta$ value of 10° (see Figure 5). The reflection appearing in the angular region is from the (200) plane and is attributable to the interlayer distance. One of the two immiscible solid phases was the resulting phase of the solid solution, and the other was

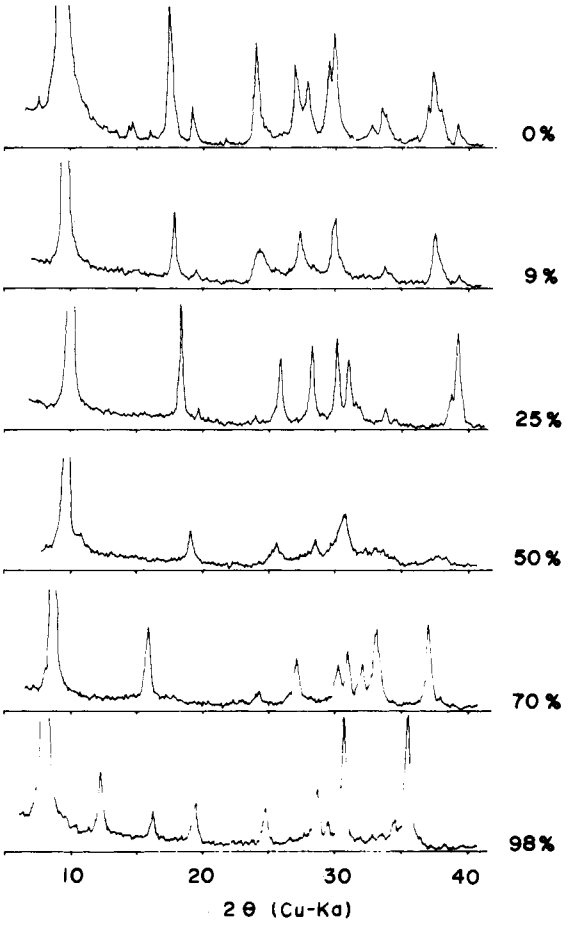


**Figure 4.** X-ray powder diffraction patterns of the solid in potassium ion exchange process. Numerals represent the percent uptake of potassium ion.

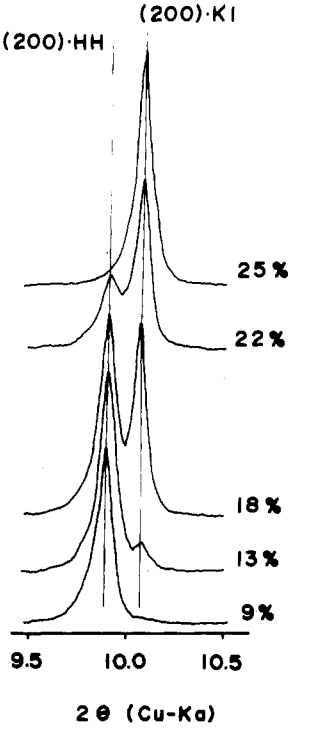


**Figure 5.** Detailed patterns of the reflections corresponding to the interlayer distance in the region of 0–25% conversion. Numerals represents the percent uptake.

a one-fourth-exchanged phase (designated phase K1) with a contracted interlayer distance of 8.6 Å and a decreased amount of hydrated water. The ratio of the latter phase increased as the

(21) Shannon, R. D.; Prewitt, C. T. *Acta Cyrstallogr., Sect. B: Struct. Crystallogr. Cryst. Chem.* **1969**, *25*, 925.

Table II. X-ray Powder Diffraction Data for Phase K1

| *h k l* | $d_{calcd}$, Å | $d_{obsd}$, Å | intens |
|---|---|---|---|
| 2 0 0 | 8.62 | 8.63 | vs |
| 2 0 $\bar{2}$ | 5.93 | 5.93 | vw |
| 2 0 1 | 5.61 | 5.62 | vw |
| 4 0 $\bar{1}$ | 4.82 | 4.81 | s |
| 4 0 $\bar{2}$ | 4.49 | 4.50 | vw |
| 4 0 0 | 4.31 | 4.31 | vw |
| 4 0 $\bar{3}$ | 3.698 | 3.699 | w |
| 4 0 1 | 3.496 | 3.497 | w |
| 2 1 0* | 3.440 | 3.442 | m |
| 6 0 $\bar{1}$ | 3.151 | 3.149 | s |
| 4 0 $\bar{4}$ | 2.963 | 2.960 | m |
| 6 0 0 | 2.873 | 2.874 | s |
| 3 1 1 | 2.834 | 2.834 | vw |
| 4 0 2 | 2.806 | 2.806 | w |
| 6 0 $\bar{4}$ | 2.649 | 2.649 | w |
| 8 0 $\bar{1}$ | 2.323 | 2.323 | m |
| 6 0 $\bar{5}$ | 2.289 | 2.291 | m |
| 8 0 0 | 2.154 | 2.154 | w |
| 8 0 $\bar{5}$ | 2.056 | 2.056 | m |
| 8 0 1 | 1.951 | 1.948 | w |
| 10 0 $\bar{2}$ | 1.910 | 1.910 | w |
| 0 2 0 | 1.876 | 1.876 | m |
| 6 0 3 | 1.871 | 1.870 | w |
| 2 2 $\bar{1}$ | 1.836 | 1.836 | m |
| 10 0 $\bar{1}$ | 1.836 | | |

exchange proceeded, and the latter phase was observed alone at 25% conversion. It is not clear from the shape of the titration curve whether the region of 25–70% conversion is a one-stage process or not, but it was confirmed from the X-ray study that this region can be divided into two regions: namely, 25–50% and 50–70% conversion. Discontinuous changes in the interlayer distance were also observed in both regions; phase K1 was converted into the half-exchanged phase (phase K2) with an interlayer distance of 9.0 Å in the former region, and phase K2 was changed into the approximately three-fourths-exchanged phase (phase K3) with an interlayer distance of 9.8 Å in the latter region. Finally, the fully exchanged phase (phase K4) was formed in the region of 70–98% conversion. Differently from the cases in the other three stages of the exchange, potassium ion uptake in this range took place without a discontinuous change in interlayer distance.

In summary, the potassium ion exchange proceeds stepwise through four stages: stage I (0–25%), stage II (25–50%), stage III (50–70%), and stage IV (70–98%). A certain stage tends to change into another stage at about $n/4$ of the theoretical ion-exchange capacity ($n$ = 1, 2, 3, 4). This is reasonable from the structure of layered hydrous titanium dioxide in which four independent exchange sites exist from a chemical point of view. The changes in chemical composition and interlayer distance are summarized as follows:

stage I: $H_2Ti_4O_9 \cdot 1.2H_2O + 0.5K^+ \rightarrow$
[9.1 Å]

$$K_{0.5}H_{1.5}Ti_4O_9 \cdot 0.6H_2O + 0.5H^+ + 0.6H_2O$$
[8.6 Å]

stage II: $K_{0.5}H_{1.5}Ti_4O_9 \cdot 0.6H_2O + 0.5K^+ \rightarrow$
[8.6 Å]

$$KHTi_4O_9 \cdot 0.5H_2O + 0.5H^+ + 0.1H_2O$$
[9.0 Å]

stage III: $KHTi_4O_9 \cdot 0.5H_2O + 0.4K^+ + 0.7H_2O \rightarrow$
[9.0 Å]

$$K_{1.4}H_{0.6}Ti_4O_9 \cdot 1.2H_2O + 0.4H^+$$
[9.8 Å]

stage IV: $K_{1.4}H_{0.6}Ti_4O_9 \cdot 1.2H_2O + 0.6K^+ + H_2O \rightarrow$
[9.8 Å]

$$K_2Ti_4O_9 \cdot 2.2H_2O + 0.6H_2O$$
[10.9 Å]

Figure 6 gives the approximate ratio of the above mentioned phases as a function of the loading, which is calculated by the relative intensities of the (200) reflection.

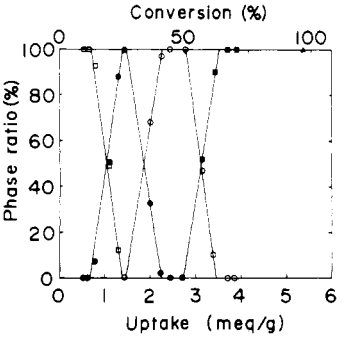


**Figure 6.** Approximate ratio of potassium ion exchanged phases as a function of loading: □, H form; ●, phase K1; ○, phase K2; ■, phase K3; ▲, phase K4.

Table III. X-ray Powder Diffraction Data for Phase K2

| *h k l* | $d_{calcd}$, Å | $d_{obsd}$, Å | intens |
|---|---|---|---|
| 2 0 0 | 9.05 | 9.07 | vs |
| 2 0 $\bar{1}$ | 8.21 | 8.20 | w |
| 3 0 $\bar{1}$* | 6.01 | 6.01 | vw |
| 1 0 $\bar{2}$* | 5.99 | | |
| 4 0 $\bar{1}$ | 4.63 | 4.63 | m |
| 2 1 0* | 3.480 | 3.486 | m |
| 2 1 $\bar{2}$* | 3.121 | 3.122 | m |
| 6 0 $\bar{1}$ | 3.118 | | |
| 3 1 1 | 2.983 | 2.978 | w |
| 0 0 4 | 2.905 | 2.905 | m |
| 1 0 $\bar{5}$* | 2.382 | 2.379 | w |
| 3 0 $\bar{5}$* | 2.378 | | |
| 6 1 $\bar{2}$* | 2.350 | 2.349 | vw |
| 8 0 $\bar{3}$ | 2.211 | 2.209 | w |
| 4 1 3* | 2.159 | 2.159 | vw |
| 8 1 1* | 1.985 | 1.986 | w |
| 0 2 0 | 1.885 | 1.885 | m |

Table IV. X-ray Powder Diffraction Data for Phase K3

| *h k l* | $d_{calcd}$, Å | $d_{obsd}$, Å | intens |
|---|---|---|---|
| 2 0 0 | 9.84 | 9.85 | vs |
| 2 0 $\bar{2}$ | 6.02 | 6.03 | vw |
| 2 0 1 | 5.97 | 5.97 | vw |
| 4 0 $\bar{1}$ | 5.57 | 5.57 | s |
| 4 0 0 | 4.92 | 4.94 | w |
| 2 0 2 | 3.976 | 3.973 | vw |
| 4 0 1 | 3.836 | 3.834 | vw |
| 1 1 0 | 3.714 | 3.712 | w |
| 3 1 $\bar{1}$ | 3.360 | 3.361 | w |
| 6 0 0 | 3.279 | 3.277 | m |
| 3 1 0 | 3.276 | | |
| 4 0 2 | 2.986 | 2.983 | w |
| 3 1 1 | 2.945 | 2.947 | m |
| 5 1 $\bar{1}$ | 2.875 | 2.880 | m |
| 6 0 1 | 2.789 | 2.789 | m |
| 8 0 $\bar{2}$ | 2.783 | | |
| 1 1 $\bar{3}$ | 2.691 | 2.693 | s |
| 8 0 $\bar{1}$ | 2.687 | | |
| 4 0 $\bar{5}$ | 2.415 | 2.419 | s |
| 6 0 $\bar{5}$ | 2.367 | 2.366 | vw |
| 8 0 1 | 2.183 | 2.182 | m |
| 10 0 $\bar{4}$ | 2.131 | 2.128 | w |
| 6 0 $\bar{6}$ | 2.007 | 2.010 | m |
| 10 0 0 | 1.967 | 1.966 | w |
| 8 0 $\bar{6}$ | 1.935 | 1.932 | w |
| 0 2 0 | 1.891 | 1.890 | m |
| 2 2 0 | 1.857 | 1.856 | w |
| 12 0 $\bar{3}$ | 1.856 | | |
| 12 0 $\bar{4}$ | 1.831 | 1.830 | vw |

**Variation in Lattice Constants during the Ion-Exchange Process.** Figure 7 summarizes the chemical compositions and lattice constants of the solid phases that appeared in the ion-exchange process. The lattice constants for phase K2 might not be very accurate because the crystallinity was relatively poor.

The values for the $b$ and $c$ axes are almost constant, indicating the host framework was not destroyed during the process. The

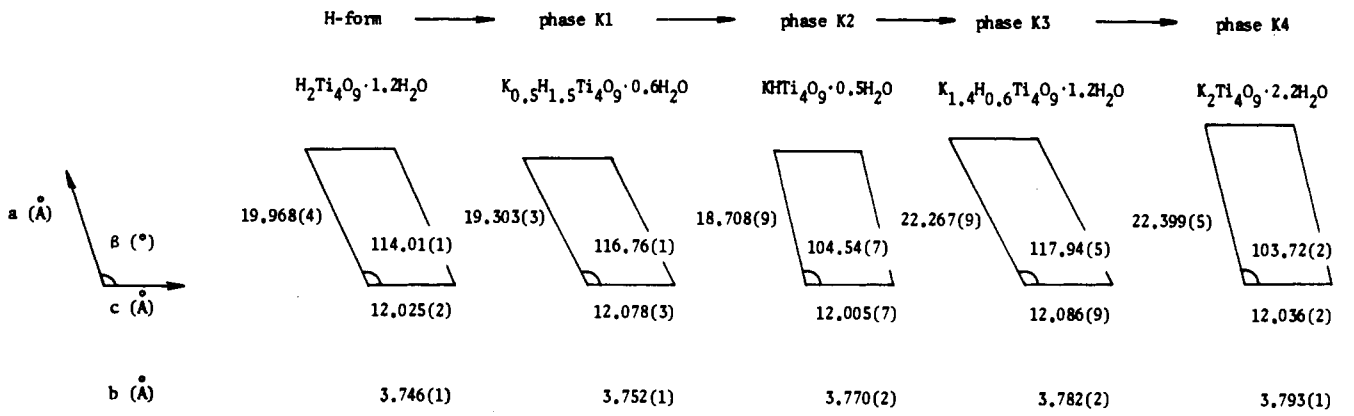


**Figure 7.** Variation in chemical composition and lattice constants in the potassium ion exchange process. The *b* axis is perpendicular to the figure.

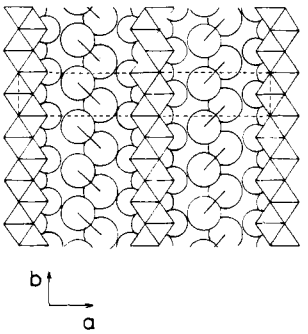


**Figure 8.** Model for arrangement of potassium ion and water molecule in interlayer spaces of phase K4 (projection along (001)): larger circle, potassium ion or water molecule; smaller circle, oxygen on the surface of the layer.

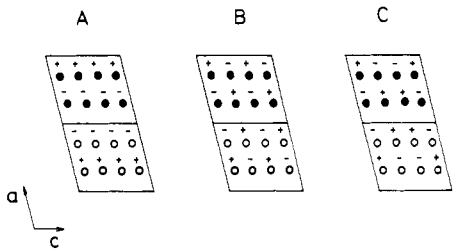


**Figure 9.** Models for a mode of the tilt of the sites: $^{+}\bullet$, $y = {}^1/_2 + \delta$; $^{-}\bullet$, $y = {}^1/_2 - \delta$; $^{+}$O, $y = 0 + \delta$; $^{-}$O, $y = 0 - \delta$.

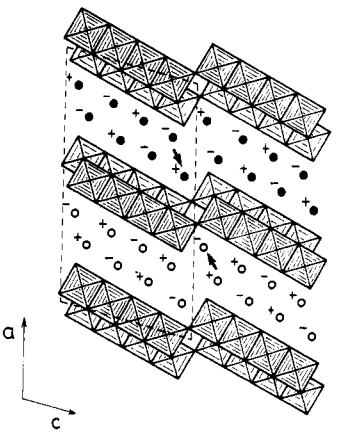


**Figure 10.** Idealized representation of the structural model of phase K4: $^{+}\bullet$, $y = {}^1/_2 + \delta$; $^{-}\bullet$, $y = {}^1/_2 - \delta$; $^{+}$O, $y = 0 + \delta$; $^{-}$O, $y = 0 - \delta$.

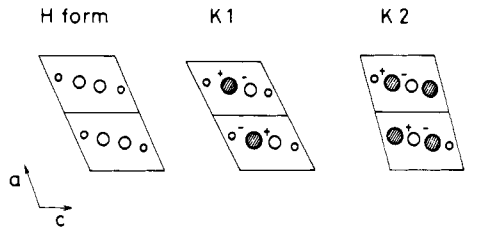


**Figure 11.** Schematic explanation for formation of phases K1 and K2: shaded circle, potassium ion; open larger circle, hydronium ion; open smaller circle, proton. The symbols "+" and "–" represent that the interlayered species are shifted from the levels at $y = 0$ and ${}^1/_2$.

value of the $\beta$ angle as well as that of the *a* axis is dependent on the degree of exchange. This fact means that the ion exchange proceeds accompanied by a shift of neighboring sheets along the *c* axis in addition to a change in interlayer distance. The indices of powder X-ray data for phases K1, K2, K3, and K4 are given in Tables II–V. The data for phases K1, K2, and K4 couldnot be indexed as a *C*-base-centered monoclinic lattice although layered hydrous titanium dioxide has a *C*-base-centered lattice. The reflections designated by an asterisk in the tables are forbidden ones. This means that a change in lattice type, from a *C*-base-centered monoclinic lattice to a primitive one, occurred during the process.

There are two possibilities for such a change: (i) a change in the host framework itself, i.e., a change in the $[Ti_4O_9^{2-}]_n$ sheet structure; (ii) a change in the arrangement of only potassium ions and water molecules while the host framework keeps a *C*-base-centered lattice. The first one is caused by a shift of neighboring sheets along the *b* axis with respect to each other. However, this change is unlikely because the reflection from the (010) plane was not observed, which must have a considerable intensity by such a shift of the sheets. In the second type, the forbidden reflections are attributable to the contribution from potassium ions and/or water molecules. We can semiquantitatively estimate the possible arrangements of potassium ions and water molecules in the interlayer space by using the indices and intensities of the forbidden reflections.

**Structural Model for the Fully Exchanged Phase.** Phase K4 has the following distinctive features compared with the other three solid phases: (i) a largely expanded interlayer distance of 10.9 Å; (ii) a double number of interlayered species, potassium ions and water molecules, in comparison with the case of potassium tetratitanate, which is reflected from the fact that the chemical formula can roughly be represented as $K_2(H_2O)_2Ti_4O_9$; (iii) several forbidden reflections with indices of $h1l$ ($h = 2n$) as given in Table V.

Facts i and ii suggest that potassium ions and water molecules are arranged in a double row in an interlayer space. A possible explanation of fact iii is that the double row is tilted with respect to the (010) plane and the tilting directions are opposite between the adjacent interlayer spaces (see Figure 8). In this case, these sites must be statistically occupied by potassium ions and water molecules since (100) and (010) reflections were not observed.

We can put forward three tentative models for a mode of the tilt as shown in Figure 9. In order to select the most likely one from these models, they were simulated by calculating the structure factors such as $F(210)$, $F(410)$, $F(\bar{4}11)$, $F(\bar{4}13)$, $F(412)$, and $F(611)$. In the process of calculation, we omitted the con-

**Table V.** X-ray Powder Diffraction Data for Phase K4

| *h k l* | $d_{calcd}$, Å | $d_{obsd}$, Å | intens |
|---|---|---|---|
| 2 0 0 | 10.88 | 10.85 | vs |
| 2 0 $\bar{1}$ | 9.12 | 9.11 | w |
| 2 0 1 | 7.16 | 7.16 | s |
| 4 0 $\bar{1}$ | 5.45 | 5.44 | m |
| 4 0 0 | 5.44 | | |
| 4 0 1 | 4.54 | 4.54 | m |
| 2 0 $\bar{3}$ | 3.981 | 3.983 | w |
| 0 0 3 | 3.897 | 3.902 | vw |
| 6 0 $\bar{1}$ | 3.723 | 3.726 | w |
| 6 0 0 | 3.627 | 3.623 | w |
| 2 1 0* | 3.582 | 3.582 | m |
| 4 0 2 | 3.581 | | |
| 6 0 1 | 3.252 | 3.252 | vw |
| 4 1 $\bar{1}$* | 3.113 | 3.113 | m |
| 4 1 0* | 3.111 | | |
| 6 0 $\bar{3}$ | 3.039 | 3.040 | w |
| 0 0 4 | 2.923 | 2.920 | s |
| 2 0 4 | 2.669 | 2.670 | w |
| 4 1 $\bar{3}$* | 2.610 | 2.610 | w |
| 4 1 2* | 2.604 | | |
| 8 0 $\bar{3}$ | 2.530 | 2.528 | s |
| 8 0 1 | 2.521 | | |
| 6 1 1* | 2.469 | 2.470 | vw |
| 4 0 $\bar{5}$ | 2.361 | 2.361 | vw |
| 6 0 $\bar{5}$ | 2.220 | 2.219 | vw |
| 10 0 2 | 2.219 | | |
| 2 0 5 | 2.182 | 2.182 | m |
| 10 0 $\bar{3}$ | 2.127 | 2.128 | m |
| 2 0 $\bar{6}$ | 2.002 | 2.003 | vw |
| 10 0 $\bar{4}$ | 1.985 | 1.985 | w |
| 4 0 5 | 1.984 | | |
| 0 2 0 | 1.896 | 1.896 | m |
| 12 0 $\bar{2}$ | 1.861 | 1.862 | m |
| 12 0 $\bar{1}$ | 1.860 | | |

tribution from the host framework, assuming that it keeps a *C*-base-centered lattice. The initial coordinates of potassium ions and water molecules were derived by symmetrically splitting the coordinates of thallium ions in the thallium tetratitanate into two,[12] as follows:

$$x_i = x0_i \pm \delta_x$$

$$y_i = y0_i \pm \delta_y$$

$$z_i = z0_i \pm \delta_z$$

where $[x_i, y_i, z_i]$ is a new coordinate of the $i$th potassium ion or water molecule, $[x0_i, y0_i, z0_i]$ is that of the $i$th thallium ion in the thallium tetratitanate, and $\delta_x$, $\delta_y$, and $\delta_z$ are variables. The observed reflections have intensities in the order of $I_{210} < I_{410,\bar{4}11} > I_{412,\bar{4}13} > I_{611}$. Model B in Figure 9 gives a satisfactory agreement between the calculated and observed data at $\delta_x \sim 0.07$, $\delta_y \sim 0.25$, and $\delta_z \sim -0.02$. These values are reasonable because the overlap of neighboring atoms is negligible. Figure 10 shows the idealized representation of the structure of this phase.

## Discussion

**Potassium Ion Exchange.** The ion exchange proceeds stepwise via several immiscible solid phases. Such a process is characteristic for inorganic ion exchangers with layer structure, e.g. crystalline zirconium phosphate.[22] The cation shows a tendency to be exchanged in a higher pH region on this material than on crystalline zirconium phosphate.[22,23] This may be related to the nature of the exchange group, namely Ti–O–H and P–O–H.

The potassium ion exchange process consists of four stages. Stage IV is a one-phase process, and the other three are two-phase processes. In a two-phase process, two solid phases coexist; one is a poorly exchanged phase and the other is a more richly exchanged phase. A similar phenomenon is usually observed in other inorganic ion exchangers with layer structure such as crystalline zirconium phosphate and related materials.[22,24,25] The ion exchange proceeds at a constant pH value in those cases, and this is explained in terms of the phase rule.[2,26,27] In the case of layered hydrous titanium dioxide, however, such a condition was satisfied only in stage I. The pH value increased gradually as the ion exchange progressed in stages II and III. This disagreement with the phase rule can probably be explained by the fact that phases K2 and K3 have a wide range of solubility. It can be seen from Figure 6 that the solid solution was formed around 50% and 70% conversion. On the other hand, phase K1 has a relatively narrow solubility range, which makes the ion exchange in stable I take place at a constant pH value.

**Structural Interpretation.** Layered hydrous titanium dioxide has four independent exchange sites: two hydronium ions and two hydroxylated protons. In stage I of the potassium ion exchange process, the moles of potassium ions incorporated were approximately equal to the moles of hydrated water released from the lattice. On the other hand, the water content was kept unchanged in stage II. These facts mean that the ingoing ions first replace one of two hydronium ions (stage I) and then one of two hydroxylated protons (stage II).

The X-ray patterns for phases K1 and K2 exhibit forbidden reflections. In a *C*-base-centered monoclinic lattice ($C2/m$), the reflections allowed are restricted to be $h + k = 2n$ and the equivalent coordinates in the lattice are $(x, y, z)$ and $(x + {}^1/_2, y + {}^1/_2, z)$. In the X-ray pattern of phase K1, only the (210) reflection was observed as an extraordinary reflection and $h0l$ ($h = 2n + 1$) reflections did not appear. This means that the *C*-base-centered relationship is destroyed for the $y$ coordinates of certain atoms while such relationships are maintained for $x$ and $z$ coordinates. According to the discussion in the Results and Analysis, forbidden reflections are attributable to the contributions from the interlayered species. In Figure 11 is shown the possible arrangement of the interlayered species in which the potassium ions and/or hydronium ions are shifted from the levels of $y = 0$ and ${}^1/_2$. As a result of these displacements, potassium ions may acquire a good coordination polyhedron.

In the X-ray pattern of phase K2, there appeared forbidden reflections with indices of $h0l$ ($h = 2n + 1$) besides $h1l$ ($h = 2n$) reflections. This indicates that the relationships for $x$ and $z$ coordinates were also not maintained. A possible model is also shown in Figure 11. This arrangement is considered to be due to a tendency to avoid the proximity of potassium ions in and between interlayer spaces.

The occupation of the third and fourth sites brings about the proximity of potassium ions, which introduces the instability by the electrostatic repulsion. Phases K3 and K4, therefore, contain hydrated water in interlayer space to shield potassium ions mutually.

There may exist another possible way in which potassium ions and water molecules are accommodated in phases K1 and K2. Complete solution to this problem must await further study.

**Comments on the Structural Model for the Fully Exchanged Phase.** The configuration of interlayered species in phase K4 is very unique. The tilt of the double row is considered to be caused by the fact that this phase must accommodate relatively large interlayered species, potassium ions ($r$ = 1.51 Å) and water molecules ($r$ = 1.40 Å).[21] This idea is confirmed by the fact that the hydration of potassium tetratitanate given in eq 2 brings about

$$\underset{[8.75\ \text{Å}]}{K_2Ti_4O_9} + 2.2H_2O \rightarrow \underset{[10.88\ \text{Å}]}{K_2Ti_4O_9 \cdot 2.2H_2O} \qquad (2)$$

an increment of interlayer distance by 2.13 Å although the water

(22) Clearfield, A. "Inorganic Ion Exchange Materials"; CRC Press: Boca Raton, FL, 1982.
(23) Kullberg, L.; Clearfield, A. *J. Phys. Chem.* **1981**, *85*, 1585.
(24) Alberti, G.; Constantino, U.; Luciani Giovagnotti, M. L. *Gazz. Chim. Ital.* **1980**, *110*, 61.
(25) Allulli, S.; Ferragina, C.; LaGinestra, A.; Massucci, M. A.; Tomassini, N. *J. Inorg. Nucl. Chem.* **1977**, *39*, 1043.
(26) Clearfield, A.; Medina, A. S. *J. Phys. Chem.* **1971**, *75*, 3750.
(27) Clearfield, A.; Duax, W. L.; Garces, J. M.; Medina, A. S. *J. Inorg. Nucl. Chem.* **1978**, *40*, 79.

molecule has a roughly spherical body of which the diameter is approximately 2.8 Å.

Another interesting feature of this phase is that the tilting direction is opposite between the adjacent interlayer spaces. This implies that there is a correlation between the adjacent spaces. If the direction is the same, the sites designated by arrows in Figure 10 become close. Such an arrangement is unstable compared with the opposite case.

**Registry No.** K, 7440-09-7; hydrous titanium dioxide, 12214-43-6.

Contribution from the Institut für anorganische Chemie, CH-3000 Bern 9, Switzerland

# Luminescence and Absorption Properties of $VCl_2$, $Mg_{1-x}V_xCl_2$, and $Cd_{1-x}V_xCl_2$ Crystals

BRIGITTE GÄLLI, ANDREAS HAUSER, and HANS U. GÜDEL*

*Received September 24, 1984*

Low-temperature luminescence and absorption spectra were recorded of $VCl_2$ doped into $MgCl_2$ and $CdCl_2$ as well as of the pure compound. There is evidence for excitation energy transfer in $VCl_2$ down to 5 K. In the diluted materials the luminescence remains unquenched up to 200 K ($Cd_{1-x}V_xCl_2$) and 250 K ($Mg_{1-x}V_xCl_2$). The broad-band $^4T_{2g} \rightarrow {}^4A_{2g}$ luminescence transition is highly structured in the diluted samples. There is multiple evidence for a Jahn–Teller effect in the $^4T_{2g}$ state with an estimated Jahn–Teller energy of the order of 200 $cm^{-1}$. Polarized absorption and Zeeman meausurements were used to assign the $^4A_{2g} \rightarrow {}^2E_g$, $^2T_{1g}$ transitions.

## 1. Introduction

The optical–spectroscopic properties of $V^{2+}$ compounds have not received as much attention as those of other divalent transition-metal ions of the first series. $V^{2+}$ has a $3d^3$ electron configuration like $Cr^{3+}$. But there is a significant difference between the two ions as far as their spectroscopic properties are concerned. In a large majority of $Cr^{3+}$ complexes the first electronically excited states are $^2E_g$ and $^2T_{1g}$. Only in an environment that produces a small ligand field is there a sufficient lowering of $^4T_{2g}$, so that broad-band luminescence from that state can be observed. There is a great deal of current interest in systems with broad-band luminescences in the near-infrared (near-IR). One of the main aims is a search for compounds that may be brought to lase with a potential for tunability.[1-3] A number of crystalline and glassy materials that exhibit broad-band $Cr^{3+}$ laser action have been developed and investigated in recent years.[1,4] In $V^{2+}$ compounds the $^4T_{2g}$ state is the lowest, potentially luminescent, state in almost all environments. $^4T_{2g} \rightarrow {}^4A_{2g}$ luminescences have been observed for $V^{2+}$ doped into $KMgF_3$, $MgF_2$, and $CsMgCl_3$ as well as for pure $CsVCl_3$.[5-7] Laser action was observed for the $MgF_2$ host lattice.[6] Encouraged by our observation that nonradiative relaxation processes could not compete with the luminescence process in $CsMg_{1-x}V_xCl_3$ up to room temperature,[7] we decided to study the spectroscopic properties of the title compounds.

The $MCl_2$ compounds used in this study all exhibit closely related layer structures, $VCl_2$ crystallizing in space group $D_{3d}^3$ and the host lattices $MgCl_2$ and $CdCl_2$ in space group $D_{3d}^5$. The M–Cl distance is 5% larger in $CdCl_2$ than in $MgCl_2$ and $VCl_2$.[8] The $MCl_6$ units are very close to octahedral, with $CdCl_2$ showing the largest trigonal compression. $VCl_2$ is an example of a two-dimensional Heisenberg antiferromagnet with a relatively large intralayer exchange coupling constant, $2J = -30$ $cm^{-1}$.[9] It undergoes a transition to three-dimensional magnetic order at 36 K,[10] but short-range magnetic order within the layers extends to much higher temperatures. Axial absorption spectra of $VCl_2$ and $Cd_{1-x}V_xCl_2$ have been reported in the literature.[11,12] In the present study we focus our attention on the $^4A_{2g} \leftrightarrow {}^4T_{2g}$ transitions, particularly in luminescence, and the fine structure in the region of $^2E_g$, $^2T_{1g}$ excitations.

**Table I.** Crystal Field Parameters Derived from the Position of the Observed Absorption Bands[a]

| compd | $D_q$, $cm^{-1}$ | $\beta$ | $K$, $cm^{-1}$ | $\zeta$, $cm^{-1}$ |
|---|---|---|---|---|
| $VCl_2$ | 935 | 0.69 | | |
| $Cd_{1-x}V_xCl_2$ | 900 | 0.70 | −210 | 100 |
| $Mg_{1-x}V_xCl_2$ | 930 | 0.72 | −270 | 100 |

[a] For crystal field calculations (weak field) the free ion energies were reduced by the factor $\beta$.

## 2. Experimental Section

**2.1. Synthesis and Crystal Growth.** $VCl_2$ was prepared by mixing stoichiometric quantities of $VCl_3$ (Cerac, 99.7%) and V powder (Merck, zur Synthese) in a quartz tube that was sealed under vacuum and slowly heated to 800 °C.[13] The few resulting platelet crystals were collected, and the grey-green powder was sublimed in a temperature gradient 1050 → 900 °C to yield another crop of green crystals. $CdCl_2$ (Pierce + Warriner suprapur) and $MgCl_2$ (Great Western Inorganics suprapur) were dried by heating them slowly under vacuum until they sublimed at 500 and 600 °C, respectively. The colder end of the tube was at 30 °C. The resulting powders were filled into quartz ampules with the desired amount of $VCl_2$ added. Single crystals were grown by the Bridgeman technique, the furnace being heated to 640 °C for the $CdCl_2$ and to 780 °C for the $MgCl_2$ host.

We always obtained crystals with a noticeable gradient in vanadium concentration due to the large difference in melting points of host and dopant. We did not succeed in growing crystals containing more than 5% of vanadium. Due to the two-dimensional structure of the crystals, plates with faces perpendicular to the crystal $c$ axis could easily be cleaved. Samples with surfaces parallel to the optical axis were difficult to obtain. The products were very hygroscopic. They were checked by means of X-ray powder diffraction. The vanadium concentration of the doped samples was measured by atomic absorption spectrometry.

(1) Kenyon, P. T.; Andrews, L.; McCollum, B.; Lempicki, A. *IEEE J. Quantum Electron.* **1982**, *QE-18* (8), 1189.
(2) Johnson, L. F.; Dietz, R. E.; Guggenheim, H. J. *Appl. Phys. Lett.* **1964**, *5* (2), 21.
(3) Johnson, L. F.; Guggenheim, H. J.; Bahnck, D. *Opt. Lett.* **1983**, *8* (7), 371.
(4) Walling, J. C.; Peterson, O. G.; Jenssen, H. P.; Morris, R. C.; Wayne O'Dell, E. *IEEE J. Quantum Electron.* **1980**, *QE-16* (12), 1302.
(5) Sturge, M. D. *Solid State Commun.* **1971**, *9*, 899.
(6) Johnson, L. F.; Guggenheim, H. J. *J. Appl. Phys.* **1967**, *38*, 4837.
(7) Hauser, A.; Güdel, H. U. *J. Lumin.* **1982**, *27*, 249.
(8) Wyckoff, R. W. G. "Crystal Structure"; Interscience: New York, 1965.
(9) Cros. C.; Niel, M.; Le Flem, G.; Pouchard, M.; Hagenmuller, P. *Mater. Res. Bull.* **1975**, *10*, 461.
(10) Hirakawa, K.; Kadowaki, H.; Ubukoshi, K. *J. Phys. Soc. Jpn.* **1983**, *52* (5), 1814.
(11) Smith, W. E. *J. Chem. Soc. A* **1969**, 2677.
(12) Kim, S. S.; Reed, S. A.; Stout, J. W. *Inorg. Chem.* **1970**, *9* (6), 1584.
(13) Hauser, A.; Falk, U.; Fischer, P.; Güdel, H. U. *J. Solid State Chem.* **1985**, *56*, 343.
(14) Moore, C. E. "Atomic Energy Levels"; National Bureau of Standards: Washington, DC, 1952.

0020-1669/85/1324-2271$01.50/0 